Journal of Power Sources 203 (2012) 48–56

Contents lists available at SciVerse ScienceDirect

Journal of Power Sources

journal homepage: www.elsevier.com/locate/jpowsour

Preparation of Pt/poly(pyrogallol)/graphene electrode and its electrocatalytic activity for methanol oxidation

Qiaofang Shi, Shaolin Mu*

Department of Chemistry, Yangzhou University, Yangzhou 225002, Jiangsu Province, China

ARTICLE INFO

Article history:
Received 24 September 2011
Received in revised form
27 November 2011
Accepted 28 November 2011
Available online 7 December 2011

Keywords:
Poly(pyrogallol)
Graphene
Pt Nanoparticles
Methanol oxidation
Electrocatalytic efficiency

ABSTRACT

Graphene (RGO) can catalyze the electrochemical oxidative polymerization of pyrogallol in the acidic solution to form poly(pyrogallol) (PPG) that has oxygen-containing functional groups in the polymer chain and a rapid charge transfer ability. Pt particles are deposited on the bare glassy carbon (GC), PPG/GC, and PPG/RGO/GC electrodes, respectively, at a constant potential of −0.20 V or −0.25 V (vs. SCE). The sizes of the Pt particles are affected by the electrodeposition potential of Pt and the kinds of the electrode material. Both PPG and graphene play an important role in improving Pt particle dispersion and suppressing the agglomeration of Pt particles. The electrocatalytic efficiency of the Pt electrodes toward methanol oxidation is affected by the amount of Pt deposited on the electrode, sizes of Pt particles and the kinds of the electrode material. Under the same electrodeposition potential and the same amount of Pt deposited on the electrode, the order of the electrocatalytic efficiency of the three kinds of the electrode is as follows: Pt/PPG/RGO/GC > Pt/PPG/GC > Pt/GC.

On the basis of the I_f/I_b ratio on cyclic voltammograms, the catalyst tolerance to CO poisoning is improved by PPG and graphene at the initial stage of methanol oxidation.

1. Introduction

The electrochemical oxidation of methanol has attracted considerable interest over the past decades because of its potential applications in the direct methanol fuel cell (DMFC) [1–5], which has high-energy conversion efficiency, low pollutant emission, low operating temperature and the storage convenience of a liquid fuel cell [6–10]. It is well known that platinum is a good catalyst for methanol oxidation. However, both the expensive Pt and lower electrocatalytic efficiency of the smooth pure Pt foil are critical problems, which limited its practical applications. A great deal of effort has been devoted to reducing the use of platinum and enhancing the catalytic efficiency of Pt for methanol oxidation, such as using platinum-based alloy catalysts of Pt–M (M = Ru, Pd, Co, Sn and nichrome) [11–20] and supporting materials of Ti, TiO_2, SnO_x and carbon [21–27]. This is because they have high catalytic activity to methanol oxidation, good tolerance to CO poisoning compared to pure platinum. For example, Pt–Ru and Pt–Co alloy electrodes, their electrocatalytic activities are about 196 mC mg^{-1} in terms of mass specific activity [19] and about 146 mA cm^{-2} in terms of the forward anodic peak current density [13], respectively; and the potential for the onset of carbon monoxide oxidation on the Pt–Sn alloy electrode surface is nearly 0.5 V lower than that for pure Pt and approximately 0.15 V lower than that for Pt–Ru alloy electrode [20]. Carbon materials have been used as catalyst support broadly and commercially. However, the pristine surfaces of glassy carbon (GC) and carbon nanoparticles are relatively inert and difficult to support Pt particle dispersion homogeneously [28,29], which often results in the agglomeration of nanoparticles, and hence affects the catalytic efficiency of Pt for methanol oxidation. It was found that the presence of conducting polymer films of polypyrrole [23,25,30–32], polyaniline [14,33–35], poly(*o*-phenylenediamine) [36,37], and polyindole [38] on the electrode surface plays an important role in improving the dispersion and stability of the nanoparticles and furthermore enhancing the catalytic efficiency of Pt nanoparticles for methanol oxidation. In addition, some authors reported that oxygen-containing functional groups on the support provide the sites for nanoparticle anchoring [39,40], increase the metal dispersion [41,42] and make the electrochemical oxidation potential of methanol shift toward less positive values [43].

Graphene sheet has high conductivity and large specific surface area, so which is a suitable supporting material for loading Pt nanoparticles. In addition, several oxygen-containing groups are present in graphene. The graphene-supported Pt electrodes exhibited a good performance for methanol oxidation [44–46] and were observed to be significantly less susceptible to CO poisoning than the traditional catalyst systems [47].

Pyrogallol with three hydroxyl groups can be polymerized electrochemically on a GC electrode to form poly(pyrogallol) (PPG) with a stable water-insoluble film [48]. However, its polymerization rate

* Corresponding author. Tel.: +86 514 87975590x9413; fax: +86 514 87975244.
E-mail address: slmu@yzu.edu.cn (S. Mu).

0378-7753/$ – see front matter © 2011 Elsevier B.V. All rights reserved.
doi:10.1016/j.jpowsour.2011.11.077

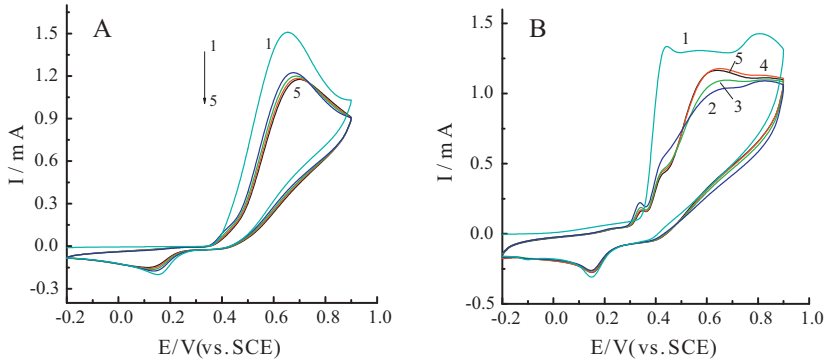

Fig. 1. Cyclic voltammograms of pyrogallol in a solution containing 50 mM pyrogallol and 0.20 M H_2SO_4, (A) GC electrode, (B) RGO/GC electrode, curves: (1) first cycle, (5) fifth cycle, at a scan rate of 60 mV s^{-1}.

is very sluggish on the GC electrode. The reduced graphene oxide (RGO) or graphene exhibits a good catalytic ability to some species [49] and can greatly catalyze the electrochemical oxidative polymerizations of aniline, aniline derivatives and *o*-phenylenediamine [50,51]. In this case, we used graphene as a catalyst to synthesize PPG, and made Pt nanoparticles deposit on a PPG/graphene/GC electrode to form a Pt/PPG/RGO/GC electrode, which was used to investigate methanol oxidation. The experimental results indicate that poly(pyrogallol) polymerized on the graphene film has a more rapid charge transfer rate compared to that of poly(pyrogallol) polymerized on the bare GC electrode; and the Pt/PPG/RGO/GC electrode exhibits a pronounced increase in the catalytic activity for methanol oxidation and a significantly less susceptibility to CO poisoning compared to that of the Pt/GC electrode. The reason for the effect of both PPG and RGO on the electrocatalytic oxidation of methanol is discussed in this report.

2. Experimental

Pyrogallol and other chemicals were of analytical reagent grade, and were purchased from Sinopharm Chemical Reagent Co., Ltd. in Shanghai. Doubly distilled water was used to prepare all aqueous solutions. A GC disk electrode (3 mm diameter) was polished with alumina slurry of 0.5 μm diameter on a polishing cloth and then sonicated in a distilled water bath for 15 min before use.

Graphene oxide (GO) nanosheets were prepared from natural graphite powders by a modified Hummer's method [52]. Aqueous dispersion of pristine GO sheets (0.05 wt.%) was prepared by sonicating for 90 min. A 5 μl aqueous dispersion of GO sheets was dropped on a GC disk that was then allowed to dry at 40 °C to form a GO/GC electrode. The GO/GC electrode was reduced at −1.0 V for 90 min in a 0.30 M phosphate buffer of pH 4.15 to form a graphene/GC electrode (i.e. RGO/GC electrode) [49–51]. A traditional three-electrode system, consisting of a GC or a RGO/GC working electrode, a platinum foil counter electrode and a saturated calomel reference electrode (SCE), was used for the electrochemical experiments that were performed on a CHI 407 workstation.

The electrochemical polymerization of pyrogallol in the acidic solution was performed using cyclic voltammetry between −0.20 and 0.90 V. Five cycles were used for the preparation of poly(pyrogallol) (PPG) that was deposited on a GC electrode or on a RGO/GC electrode. After polymerization, the PPG electrodes were washed with distilled water and then were cycled between −0.20 and 0.80 V for five cycles in 0.20 M H_2SO_4 solution. The purpose is to remove pyrogallol in the polymer film. These polymer electrodes were used for Pt electrodeposition.

Methanol oxidation was carried out in nitrogen atmosphere at 25 °C. Before electrolysis, the methanol solution was first deoxygenated by bubbling N_2 for 10 min, and then a continuous flow of nitrogen was maintained over the solution during the methanol oxidation process.

Pt electrodeposition was carried out on a PAR Model 173 potentiostat-galvanostat with a Model 179 digital coulometer, at a constant potential of −0.20 or −0.25 V (vs. SCE), in a solution consisting of 3 mM H_2PtCl_6 and 0.10 M KCl. The digital coulometer can accurately record charges during the electrodeposition process. The amount of Pt deposited on the GC disk, PPG/GC and PPG/RGO/GC electrodes was determined by total charges consumed during the electrolytic process, assuming a 100% current efficiency.

$$W_{Pt} = \frac{QM_{Pt}}{nF}$$

where n is the number of electrons for the reduction of H_2PtCl_6 to Pt, which is taken as 4. The other symbols have their usual meaning. In this work, the total charge of 1.75×10^{-2} C or 3.50×10^{-2} C was used to deposit Pt on the electrodes; the corresponding Pt loading is 125 and 250 μg cm^{-2}, respectively. The apparent surface area of the electrodes was calculated based on the GC electrode of 3 mm diameter.

The images of Pt particles deposited on GC, PPG/GC, and PPG/RGO/GC electrodes were observed by a field emission scanning electron microscope (SEM) S-4800 II FE-SEM. The impedance measurements of poly(pyrogallol) films were performed on an Autolab instrument. Frequency sweeps extended from 10^4 to 0.01 Hz using a sinusoidal perturbation signal of 10 mV, peak-to-peak. The infrared reflection spectra of polymer were measured using a Nicolet 670-FT-IR spectrometer.

3. Results and discussion

3.1. Synthesis and electrochemical properties of poly(pyrogallol)

Fig. 1A and B is the cyclic voltammograms of pyrogallol in a solution containing 50 mM pyrogallol and 0.20 M H_2SO_4 at a GC electrode and a RGO/GC electrode, respectively. An oxidation peak at 0.65 V occurs on the first cycle (curve 1) in Fig. 1A, which is caused by pyrogallol oxidation that results in the polymerization of pyrogallol to form PPG film on the GC electrode surface. However, for the second cycle, this peak shifts toward the positive potential direction and its peak current decreases pronouncedly compared to that of the first cycle, indicating that the conductivity of the polymer film is relatively low. After the second cycle, the peak current decreases slowly with an increasing number of cycles. Fig. 1B shows two oxidation peaks at 0.44 and 0.81 V on the first cycle, in which the first oxidation peak is attributed to pyrogallol oxidation, and then the oxidized species are oxidized further to form PPG with a shift of the sweeping potential toward the more positive

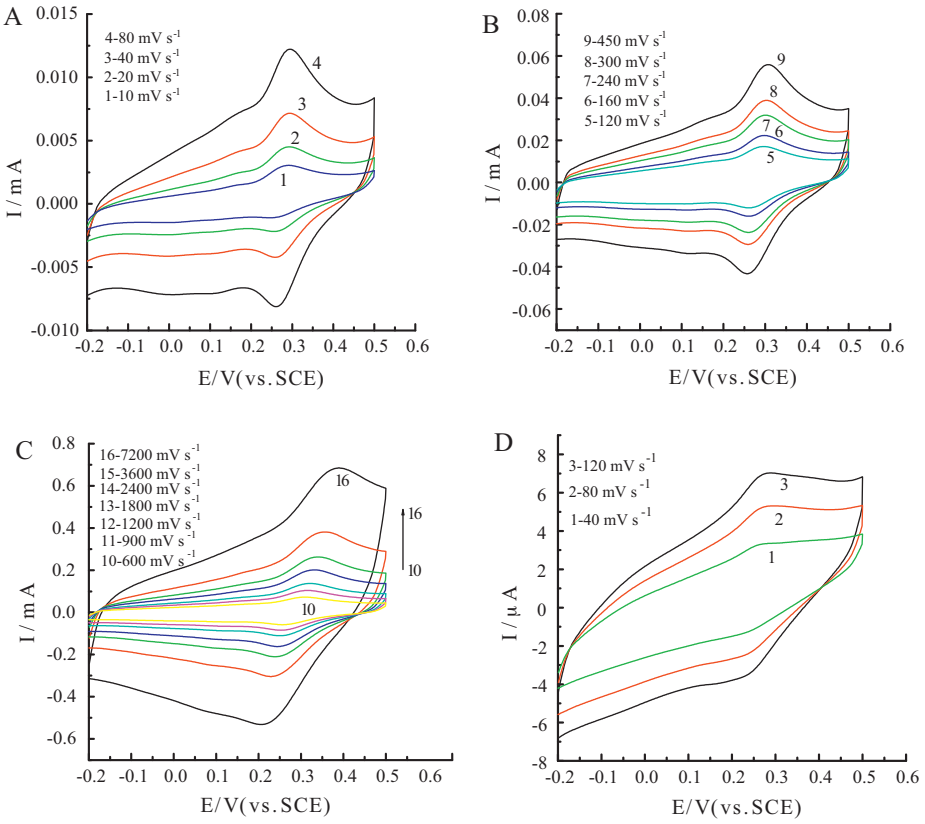

Fig. 2. Cyclic voltammograms of poly(pyrogallol) at various scan rates, (A–C) polymerized on a RGO/GC electrode, (D) polymerized on a GC electrode, in a 0.30 M Na_2SO_4 solution with pH 5.0.

potentials. This electrode is labeled PPG/RGO/GC. The anodic peak potential of pyrogallol shifts from 0.65 V at the GC electrode (curve 1 in Fig. 1A) to 0.44 V at the RGO/GC electrode (curve 1 in Fig. 1B). This is the electrocatalytic oxidation characteristic of a species for cyclic voltammetry, which is caused by RGO due to the presence of the free radical [50]. The free radical in RGO is originated from GO nanosheets due to the oxidation of the graphite powder for the preparation of GO nanosheets; after GO reduction, the free radical is still retained in RGO. The free radicals in both GO and RGO were detected by the ESR measurement [50]. The increase in the anodic peak current with an increasing number of cycles after the second cycle is observed in Fig. 1B, which is quite different from that in Fig. 1A. This difference is also caused by RGO that catalyzes the oxidative polymerization of pyrogallol. The polymerization process of pyrogallol at the RGO/GC electrode is presumed to be the following:

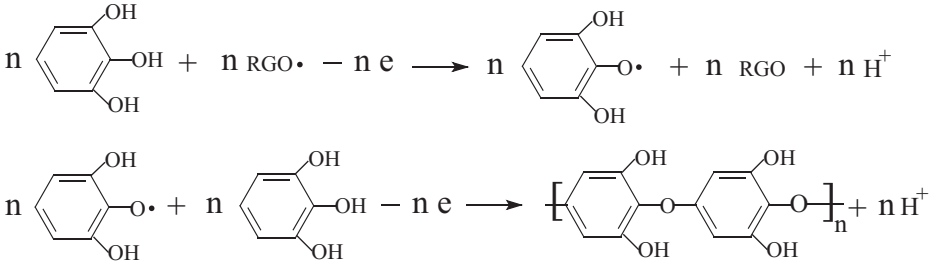

Fig. 2A–C and D shows the cyclic voltammograms of a PPG/RGO/GC electrode and a PPG/GC electrode at various scan rates, respectively, in a 0.30 M Na_2SO_4 solution of pH 5.0. A well-defined redox couple occurs in Fig. 2A–C in a scan rate range of 0.01–7.20 V s^{-1}, which demonstrates that PPG polymerized on a RGO/GC electrode has a rapid charge transfer rate; and the electrode reaction is still controlled by mass transfer at such fast scan rate. Fig. 2D shows the cyclic voltammograms of PPG/GC electrode at different scan rates. There is no well-defined reduction peak in Fig. 2D, indicating that it has a slow charge transfer rate. The reason for the rapid charge transfer rate of PPG polymerized on a RGO/GC electrode is caused by RGO because it has a high conductivity and rapid charge transfer ability.

Fig. 3A and B shows the impedance plots of the PPG/GC and PPG/RGO/GC electrodes in 0.50 M H_2SO_4 solution at 0.50 V, respectively. In a wide frequency regime, no any trace for the formation of the semicircle is observed in Fig. 3A, indicating that the charge transfer resistance R_{ct} of the PPG/GC electrode is very large. Therefore, the PPG/GC electrode is kinetically rather sluggish. However, the R_{ct} of the PPG/RGO/GC electrode can be estimated to be about 4 kΩ, that is lower than that of the PPG/GC electrode. The possible reasons are that the amount of PPG polymerized on the RGO/GC electrode is greater than that of PPG polymerized on the GC electrode due to the electrocatalytic oxidative polymerization of pyrogallol by graphene, and PPG polymerized on the RGO/GC electrode has a large surface area and

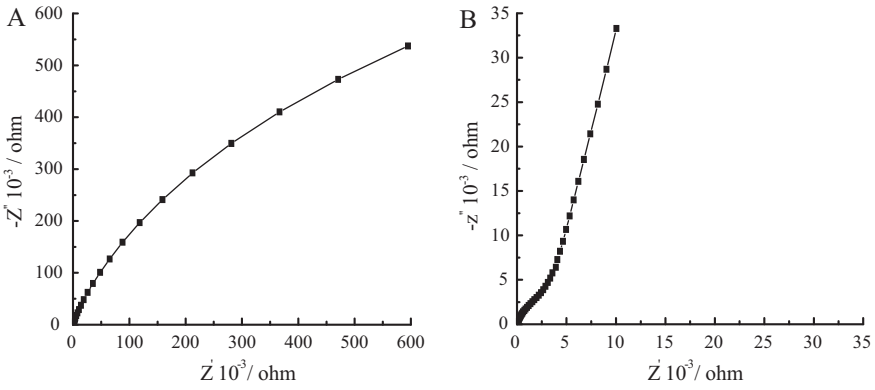

Fig. 3. The impedance plots: (A) PPG/GC and (B) PPG/RGO/GC in 0.50 M H_2SO_4 solution.

rapid charge transfer ability. These factors resulted in the R_{ct} of the PPG/RGO/GC electrode is smaller than that of PPG/GC electrode. Furthermore the Warburg impedance in the lower frequency regime is observed in Fig. 3B. The latter result demonstrates that the reaction of the PPG/RGO/GC electrode is controlled by mass transfer, that is, the PPG/RGO/GC electrode is kinetically more rapid than that of the PPG/GC electrode. This result is in good agreement with that of cyclic voltammograms in Fig. 2.

Curves 1 and 2 in Fig. 4 are the IR spectra of PPG/GC and PPG/RGO/GC, respectively. The main reflection peaks are discussed here. A broad band centered near 3500 cm^{-1} is attributed to the hydrogen-bonded OH stretching vibrations of phenols. A peak at 1610 cm^{-1} on curve 1 and 1614 cm^{-1} on curve 2 are assigned to C=C stretching vibrations of the benzene ring. A peak at 1460 cm^{-1} in curve 2 would be attributed to C–O–H deformation vibrations in carboxylic acids. A peak at 1330 cm^{-1} on curves 1 and 2 would be assigned to OH deformation in phenols because phenols absorb near 1350 cm^{-1} due to the OH deformation and give a second broader, stronger band due to C–OH stretching near 1200 cm^{-1} [53]. Therefore, a peak at 1176 cm^{-1} on curve 2 is attributed to C–OH stretching vibrations. To assign the contribution of the peak at 986 cm^{-1} on curve 1 and at 993 cm^{-1} on curve 2, the IR spectrum of pyrogallol was measured in our work, in which a very strong sharp peak appears at 1000 cm^{-1}. Therefore, both peaks at 986 and 993 cm^{-1} in Fig. 4 should be attributed to C–OH stretching vibrations. Fig. 4 indicates that the IR spectrum on curve 2 is similar to that on curve 1, but there is small difference between them such as the IR signal intensity of PPG/RGO/GC (curve 2) is stronger than that of PPG/GC (curve 1), and two new peaks at 1176

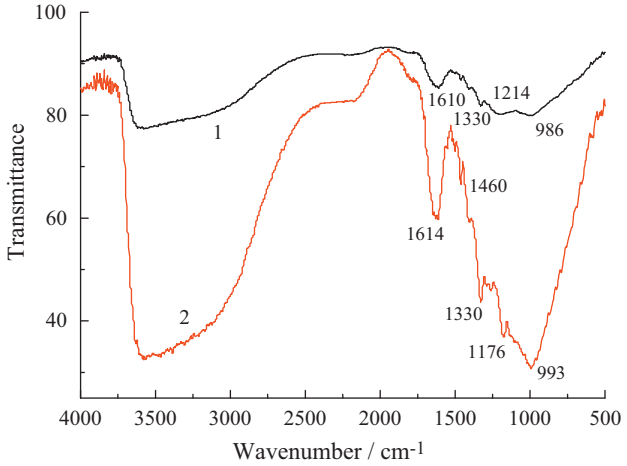

Fig. 4. IR spectra of PPG/GC (1) and PPG/RGO/GC (2).

and 1460 cm^{-1} occur on curve 2. This difference is caused by the amount of PPG polymerized on the RGO/GC electrode, which is larger than that of PPG polymerized on the GC electrode because the oxidative polymerization of pyrogallol was catalyzed by RGO; and RGO was contained in the PPG/RGO/GC electrode. It is clear that the oxygen-containing functional groups are contained in the PPG/GC and PPG/RGO/GC electrodes.

3.2. *Effect of the electrode material and applied potential on images of Pt particles*

The images of Pt particles on GC, PPG/GC, and PPG/RGO/GC electrodes are shown in A, B–C, and D of Fig. 5, respectively. The electrodeposition of Pt was performed at −0.20 V; and the total charge for the Pt electrodeposition on each electrode is 3.50×10^{-2} C, which is corresponding to the Pt loading of 250 μg cm^{-2}. The SEM images in Fig. 5 reveal a fact that Pt particles deposited on each supporting matrix are constructed of spherical particles with different sizes. The diameters of Pt particles are about 400 nm to 1 μm in Fig. 5A, 400 nm to 800 nm in Fig. 5B, and 200 nm to 300 nm in Fig. 5D. Clearly, the sizes of Pt particles are affected by the electrode material for Pt deposition. Among them, the sizes of Pt particles deposited on the PPG/RGO/GC surface are the smallest due to the synergetic effect of PPG and graphene composite film on the GC surface. Graphene sheet has a large specific surface area and exhibits a unique structure of two-dimensional structure, which is advantageous to formation of PPG film with large surface area and deposition of Pt particles. As a result, the sizes of Pt particles on the PPG/RGO/GC electrode are smaller than those of Pt particles on the PPG/GC electrode. Fig. 5C shows the image of a large Pt particle in Fig. 5B. Clearly, the large Pt particle consists of a numerous small spherical particles with an average diameter of about 30 nm. These small particles are aggregated together to form a large Pt particle. The result from Fig. 5D demonstrates that the PPG/RGO composite film plays an important role in improving Pt particle dispersion and suppressing aggregation of Pt particles due to the presence of the oxygen-containing functional groups that are sites for nanoparticle anchoring [39,43].

The images of Pt particles deposited on GC, PPG/GC, and PPG/RGO/GC electrodes are shown in A, B, and C of Fig. 6, respectively; they were obtained at −0.25 V for the electrodeposition of Pt. The total charge for Pt deposition is also 3.50×10^{-2} C. Fig. 6 shows the images of the electrode surface consisting of Pt flakes with different diameters and lengths. The size of Pt flakes deposited on the PPG/RGO/GC electrode (Fig. 6C) is still smallest among the three electrodes; its reason is the same as that explained previously. Fig. 6C shows that the flakes have an average diameter of about 40 nm with lengths varying from 60 to 120 nm. The sizes of Pt particles deposited on three electrodes in Fig. 6 are much smaller

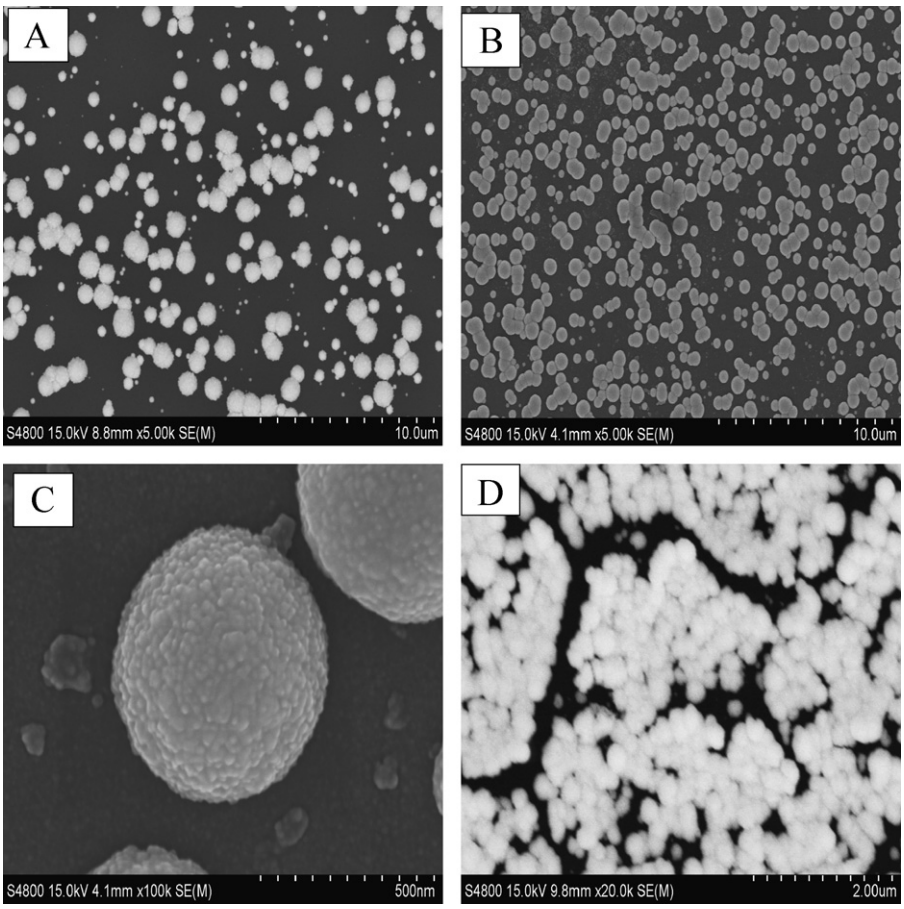

Fig. 5. Images of Pt particles deposited on (A) GC, (B, C) PPG/GC, (D) PPG/RGO/GC electrodes, at a deposition potential of −0.20 V, Pt loading of 250 μg cm^{-2}.

than those of Pt particles deposited on the corresponding electrode in Fig. 5, indicating that the sizes of Pt particles are strongly affected by the Pt deposition potential. It is well known that the reduction rate of a species increases with increasing negative potential. Thus, the deposition rate of Pt from H_2PtCl_6 reduction increases as the applied potential moves from −0.20 to −0.25 V. A faster deposition rate is favorable to accelerate the formation of Pt nuclei. As a result, the amount of Pt nuclei deposited on the electrode surface increases, which plays a significant role in suppressing nuclei growth and improving the Pt particle nuclei dispersion. Therefore, the sizes of Pt particles formed at −0.25 V are much smaller than those formed at −0.20 V. However, the particle morphology changes from spherical particles in Fig. 5 to flakes in Fig. 6, this may be attributed to the rapid formation of a large amount of Pt nuclei at −0.25 V and the increase in the non-uniformity of the electric field at the disk working electrode with increasing the applied cathodic potential because an Pt foil counter electrode is not parallel to the disk working electrode in the electrolytic cell. In that case, the Pt nuclei get together to form flakes as the electrolysis proceeds.

3.3. *Effect of the amount of Pt deposited on the catalyst efficiency to methanol oxidation*

In this section, the electrodeposition of Pt was carried out at a constant potential of −0.20 V. The electrocatalytic activity of Pt deposited on the different electrodes was characterized using cyclic voltammetry in a solution consisting of 1.0 M methanol and 0.50 M H_2SO_4; and the scan rate was set at 50 mV s^{-1}. In this work, 20 cycles for each electrode were recorded for testing the effect of potential cycles on the catalytic activity of Pt. Fig. 7A shows the cyclic voltammograms of Pt deposited on GC (curve 1), PPG/GC (curve 2), and PPG/RGO/GC (curve 3) electrodes. The amount of Pt deposited on each electrode is 125 μg cm^{-2}. Considering the change in the catalytic activity of the electrode with cycles, a cyclic voltammogram with the maximum catalytic activity is used in Fig. 7A and B for each electrode. The maximum forward anodic peak current density is observed at the 6th cycle for the Pt/GC and Pt/PPG/GC electrodes and at the 15th cycle for the Pt/PPG/RGO/GC electrode. As can be seen from Fig. 7A, the forward anodic peak current density is the smallest for the Pt/GC electrode and is the largest for the Pt/PPG/RGO/GC electrode. Fig. 7B shows the cyclic voltammograms of Pt deposited on GC (curve 1), PPG/GC (curve 2), and PPG/RGO/GC (curve 3) electrodes; the amount of Pt deposited on each electrode is 250 μg cm^{-2}. The maximum forward anodic peak current density is 15.9, 21.1, and 31.3 mA cm^{-2} appearing at the 15th cycle for the Pt/GC and Pt/PPG/GC electrodes, and at the 20th cycle for the Pt/PPG/RGO/GC electrodes, respectively. The order of the current density for three kinds of the electrode is similar to that in Fig. 7A. This is because the sizes of Pt particles are the largest on the GC electrode and the smallest on the PPG/RGO/GO electrode (Fig. 5); and furthermore, the dispersion of Pt particles on the PPG/GC and PPG/RGO/GC electrodes was evidently improved compared to the GC electrode. This indicates that PPG and RGO films play an important role in improving the dispersion of Pt particles, which leads to increasing electrocatalytic activity of Pt under the same amount of Pt deposited on the electrode. In comparison with Fig. 7A, the peak current density for each electrode in Fig. 7B is two times as large as that in Fig. 7A because the Pt loading on

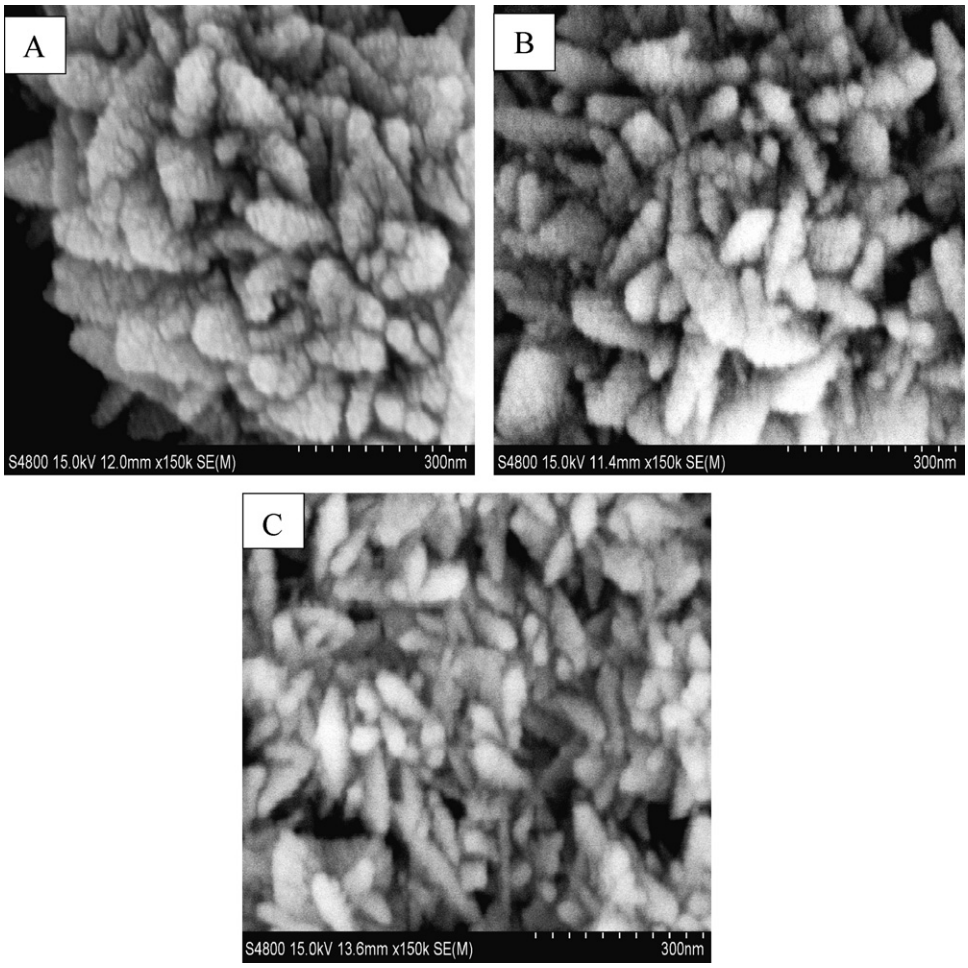

Fig. 6. Images of Pt particles deposited on (A) GC, (B) PPG/GC, (C) PPG/RGO/GC electrodes, at a deposition potential of −0.25 V, Pt loading of 250 μg cm^{-2}.

each electrode in Fig. 7B is higher than that in Fig. 7A, which has been examined by previous works [54,55]. Fig. 7B shows that the onset oxidation potential of methanol oxidation is about 0.40 V on Pt/GC and the Pt/PPG/GC electrodes and is however at about 0.30 V on the Pt/PPG/RGO/GC electrode. This difference is mainly caused by the PPG/RGO composite film that has more rapid charge transfer ability compared with PPG polymerized on the bare GC electrode as discussed previously. In addition, Fig. 7A and B shows that the peak potential of methanol oxidation for the forward scan is at 0.65 V at the Pt/PPG/RGO/GC electrode, which is a little more negative than those at the Pt/GC and Pt/PPG/GC electrodes. The values of the peak current density, peak potential, and the onset potential of methanol oxidation for the forward scan are usually used for evaluating the catalytic activity of Pt toward methanol oxidation. The results shown in Fig. 7A and B demonstrate that the order for the electrocatalytic efficiency of the three kinds of the electrode is as follows:

Pt/PPG/RGO/GC > Pt/PPG/GC > Pt/GC

Fig. 7C shows the cyclic voltammograms of the Pt/PPG/RGO/GC electrode from the 1st to 20th cycles in a solution consisting of 1.0 M methanol and 0.50 M H_2SO_4. Clearly the peak current density of methanol oxidation in the forward scan from −0.20 to 0.90 V and in the backward scan from 0.90 to −0.20 V increases with an increasing number of cycles from the 1st cycle to the 20th cycle and the oxidation peak potential shifts slightly toward the negative potential direction for the forward and backward scans with increasing cycles. This phenomenon has been observed in the previous report [33]. The reason for the peak current of methanol oxidation on the forward scan increases with an increasing number of cycles would be caused by the automatic activation of Pt particles [33] or the formation of the free radicals at the initial stage for methanol oxidation. This phenomenon was also observed on the bare platinum foil in our laboratory. The peak current on the backward scan also increases with an increasing number of cycles, which is due to the accumulation of intermediates produced in the forward scan process, which can be oxidized at lower positive potentials.

The oxidation of methanol on the Pt catalyst forms CO and other intermediate carbonaceous species, which hinder further oxidation of methanol and cause the surface poison of the Pt catalyst. Hence, the ratio of the forward anodic peak current density I_f to the backward anodic peak current density I_b, I_f/I_b, is usually used to assess the catalyst tolerance to carbonaceous species accumulation [44,56]. The change in the ratio of I_f/I_b as a function of cycles is shown in Fig. 7D for the three electrodes, which was calculated based on their forward and backward peak current densities among 20 cycles shown in Fig. 7B. For the first cycle, the I_f/I_b ratio is 1.67, 2.04, and 2.17 for the Pt/GC, Pt/PPG/GC, and Pt/PPG/RGO/GC electrodes, respectively. Obviously, the I_f/I_b ratio is the smallest for the Pt/GC electrode and is the largest for the Pt/PPG/RGO/GC electrode among the three kinds of the electrode. The reason for this is that the –OH groups are contained in PPG, and the oxygen-containing functional groups are included in graphene. They are favorable for the production of CO_2 from the oxidation of CO produced in the forward scan, which was proven by the in situ FTIR

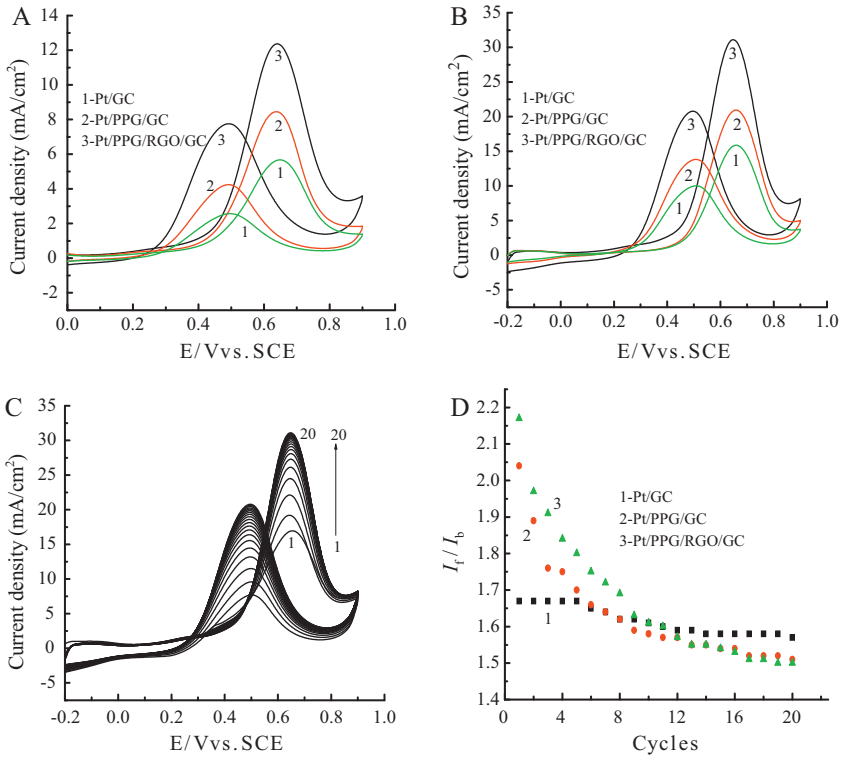

Fig. 7. Cyclic voltammograms of methanol oxidation at different Pt electrodes in a solution consisting of 1.0 M CH_3OH and 0.50 M H_2SO_4 at a scan rate of 50 mV s^{-1}, the Pt deposition potential is controlled at −0.20 V. (A) Pt loading of 125 μg cm^{-2}. (B) Pt loading of 250 μg cm^{-2}, the cyclic voltammogram with the highest forward anodic peak current density for each electrode among 20 cycles. (C) The cyclic voltammograms as a function of scan cycles, Pt loading of 250 μg cm^{-2}. (D) I_f/I_b as a function of scan cycles for different Pt electrodes, Pt loading of 250 μg cm^{-2}.

spectra during methanol oxidation [43]. Fig. 7D shows that the I_f/I_b ratio decreases with an increasing number of cycles for three kinds of the electrode, but their decay rates are different with each other, depending on the electrode material. The I_f/I_b ratio of the Pt/GC electrode changes slightly with increasing cycles, and is a little higher than that of the Pt/PPG/GC electrode after 8 cycles and higher than that of the Pt/PPG/RGO/GC electrode after 11 cycles. The small difference between the Pt/PPG/GC and Pt/PPG/RGO/GC electrodes is due to the fact that the oxygen-containing functional groups are also contained in graphene, which led to its tolerance to CO poisoning being better than that of the Pt/PPG/GC electrode. The I_f/I_b ratio of the Pt/GC electrode changes slightly with increasing cycles, which is attributable to its low peak current density of the forward scan compared to another two electrodes shown in Fig. 7B. This indicates that the change in the I_f/I_b ratio with cycles is related to the forward peak current density since the higher anodic peak current density leads to the formation of the lager amount of intermediates on the catalyst surface. The I_f/I_b ratio is 1.47 for the Pt/graphene nanosheets [44], and is 4.39 for the Pt–Ru/carbon black [45]. Clearly, the I_f/I_b ratio of the Pt/PPG/GC or Pt/PPG/RGO/GC electrode is larger than that of the Pt/graphene nanosheets due to poly(pyrogallol) with oxygen-containing functional groups; however, the I_f/I_b ratio of the Pt/PPG/RGO/GC electrode is smaller than that of Pt–Ru electrode [45]. Therefore, the Pt–Ru alloy electrode has a good tolerance to CO poisoning [45], but the I_f/I_b ratio of the carbon supported Pt–Ru electrode is smaller [19], its reason is not clear to us.

Fig. 8A shows the current densities of the three electrodes with Pt loading of 250 μg cm^{-2} as a function of time during methanol oxidation at a constant potential of 0.50 V. The Pt electrodeposition for the three electrodes was carried out at −0.20 V. Fig. 8A indicates that the current density is the largest for the Pt/PPG/RGO/GC electrode and is the smallest for the Pt/GC electrode among the three electrodes. This result is in good agreement with that shown in Fig. 7. As can be seen from Fig. 8A, a decay of the current density for methanol oxidation on the Pt/GC electrode is slower than that of the Pt/PPG/GC or Pt/PPG/RGO/GC electrode. One of reasons for this result is caused by concentration polarization at the electrode in the quiescent solution in the process of methanol oxidation; thus, the Pt/PPG/RGO/GC electrode with the largest current density is polarized more easily than that of the Pt/GC electrode with smallest current density among the three electrodes; another one is due to a decrease in the I_f/I_b of the Pt/PPG/RGO/GC electrode being faster than that of the Pt/GC electrode. From the change in the current density with time shown in Fig. 8A, the Pt/PPG/GC and Pt/PPG/RGO/GC electrodes are quite stable.

The above results show that the Pt electrode with higher amount of Pt not only exhibits the higher electrocatalytic efficiency but also improves the stability of the Pt electrodes compared with the Pt electrodes with lower amount of Pt. In this case, a Pt electrode with Pt loading of 375 μg cm^{-2} was used to study methanol oxidation, in which Pt particles were deposited on the PPG/RGO/GC electrode at −0.20 V. The result is shown in Fig. 8B, in which the maximum forward anodic peak current density is 55.7 mA cm^{-2} appearing at the 8th cycle (curve 3) that is higher than that of curve 3 in Fig. 7B; and however, the peak current density decreases with increasing number of cycles from the 8th cycle (curve 3) to the 20th cycle (curve 5) in Fig. 8B, which is different from that in Fig. 7C. The result shown in Fig. 8B demonstrates that the electrocatalytic efficiency of the electrode with Pt loading of 375 μg cm^{-2} is higher than that with Pt loading of 250 μg cm^{-2}, but its stability was suffered from a decay with an increasing number of cycles. In this case, the electrodes with Pt loading of 125 and 250 μg cm^{-2} were used in the following experiments.

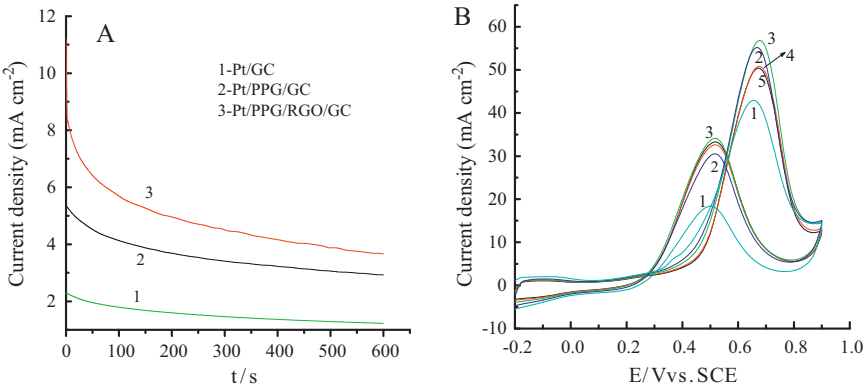

Fig. 8. (A) Chronoamperometric curves of Pt/GC (1), Pt/PPG/GC (2), and Pt/PPG/RGO/GC (3) in a solution of 1.0 M methanol and 0.5 M H_2SO_4, at 0.50 V (vs. SCE). (B) Cyclic voltammograms of methanol oxidation at the Pt/PPG/RGO/GC electrode with Pt loading of 375 μg cm^{-2} in a solution consisting of 1.0 M CH_3OH and 0.50 M H_2SO_4 at a scan rate of 50 mV s^{-1}, the Pt deposition potential is controlled at −0.20 V, curves: (1) 1st cycle; (2) 4th cycle; (3) 8th cycle; (4) 15th cycle; (5) 20th cycle.

3.4. *Effect of the Pt electrodeposition potential on the catalyst efficiency*

In this section, all Pt electrodes were prepared at a constant potential of −0.25 V. The amount of Pt deposited on each electrode is 250 μg cm^{-2}. Fig. 9A shows the cyclic voltammograms of the Pt/GC, Pt/PPG/GC, and Pt/PPG/RGO/GC electrodes, with the maximum forward anodic peak current density for each electrode among 20 cycles in the process of methanol oxidation. The maximum forward anodic peak current density for methanol oxidation is 25.6, 38.8, and 57.2 mA cm^{-2} at the Pt/GC, Pt/PPG/GC, and Pt/PPG/RGO/GC electrodes, respectively. Clearly, the order of the forward anodic peak current density for three different kinds of the electrode is same as that in Fig. 7A and B, The reason for this is discussed previously. However, the peak current density of each electrode in Fig. 9A is much higher than that in Fig. 7B for the corresponding electrode. This difference is caused by the sizes of Pt particles because the sizes of the Pt particles obtained at −0.25 V is only about one-tenth of sizes of Pt particles obtained at −0.20 V for the corresponding electrode. The maximum anodic peak current density (57.2 mA cm^{-2}) of the Pt/PPG/RGO/GC electrode with Pt loading of 250 μg cm^{-2} is close to that of the Pt–Co/PPY–MWCNT electrode (with Pt loading of 500 μg cm^{-2}) before over-oxidation, under the same experimental conditions including the composition of methanol solution and the potential scan rate [13]. The carbon supported Pt–Ru electrode showed higher electrocatalytic activity in terms of mass specific activity, but the potential scan rate of cyclic voltammetry was controlled at 100 mV s^{-1}, therefore, its result cannot be compared with our result because the potential scan rate was set at 50 mV s^{-1} in our work.

Fig. 9B shows the change in the forward anodic peak current density with an increasing number of cycles for the three kinds of the electrode. The Pt/GC electrode (curve 1) exhibits that its forward anodic peak current density increases quickly first and then slowly until the 20th cycle. The Pt/PPG/GC electrode (curve 2) is almost similar to the Pt/GC electrode in the change of the forward anodic peak current density with an increasing number of cycles. However, a maximum forward anodic peak current density occurs at the 10th to 12th cycles for the Pt/PPG/RGO/GC electrode (curve 3) and then decreases slightly with an increasing number of cycles, and finally reaches a constant value, in which the catalytic efficiency of the Pt/PPG/RGO/GC electrode decreased only 3.1% in going from the 12th cycle to the 20th cycle. In comparison with the results from Fig. 7A and B, the stability of both Pt/GC and Pt/PPG/GC electrodes was improved, which is attributed to the formation of the Pt nanoparticles and highly dispersed particles. Even though the stability of the Pt/GC electrode prepared at −0.25 V was improved, its forward anodic peak potential shifts to more positive potentials, for example, it is 0.74 V for the first cycle. However, the forward anodic peak potential of methanol oxidation for the first cycle is 0.64 V at the Pt/PPG/GC electrode and 0.63 V at the Pt/PPG/RGO/GC electrode, which were prepared under the same conditions as the Pt/GC electrode. Clearly the forward anodic peak potential of methanol oxidation at the Pt/GC electrode is much positive than those of the

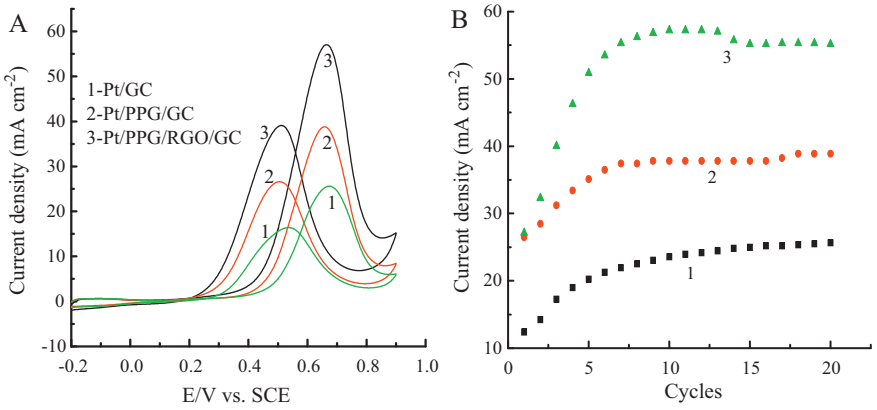

Fig. 9. (A) Cyclic voltammograms of methanol oxidation at different Pt electrodes in a solution consisting of 1.0 M CH_3OH and 0.50 M H_2SO_4 at a scan rate of 50 mV s^{-1}, with the highest forward anodic peak current density for each electrode among 20 cycles, the Pt deposition potential is controlled at −0.25 V, Pt loading of 250 μg cm^{-2}. (B) The change in the forward anodic peak current density as a function of scan cycles, (1) Pt/GC, (2) Pt/PPG/GC, (3) Pt/PPG/RGO/GC electrodes.

Pt/PPG/GC and PT/PPG/RGO/GC electrodes for the first cycle, which is caused by the polarization of the Pt/GC electrode due to the higher anodic current density.

On the basis of the results shown in Fig. 9B, the forward anodic peak current densities of both Pt/PPG/GC and Pt/PPG/RGO/GC achieve more easily the steady state compared with the Pt/GC electrode; furthermore, the time for achieving the steady state of a pure Pt foil used for methanol oxidation needs over 100 cycles under the same experimental conditions shown in Fig. 9A, indicating that the activation time of the Pt electrode is related to the electrode material. In addition, the activation of the Pt electrode used for the electrocatalytic oxidation of methanol also depends on the preparation conditions for the same electrode material such as Pt–Ru alloy electrodes, one of them prepared under the optimum conditions is more easily to achieve the steady state than other Pt–Ru electrodes during the process of methanol oxidation [19].

4. Conclusion

Graphene catalyzed the electrochemical oxidative polymerization of pyrogallol in the acidic solution to form PPG that has rapid charge transfer ability. Therefore PPG is a new electrode material. Pt particles were deposited on the GC, PPG/GC, and PPG/RGO/GC electrodes to form three kinds of the Pt electrode at a constant potential of −0.20 or −0.25 V, which were used to study methanol oxidation in 0.50 M H_2SO_4 solution. The sizes of Pt particles are strongly affected by its electrodeposition potential and the electrode materials. The electrocatalytic efficiency of the Pt electrode toward methanol oxidation increased with increasing the amount of Pt deposition and with decreasing the sizes of Pt particles, and depends on the electrode materials used for Pt deposition. The order of the electrocatalytic efficiency of the Pt electrodes toward methanol oxidation under the same amount of Pt deposited on the electrode and the same electrodeposition potential of Pt is as follows:

Pt/PPG/RGO/GC > Pt/PPG/GC > Pt/GC

This order is in good agreement with the sizes of Pt particles and the charge transfer ability of the electrodes because Pt particles with minimum sizes were obtained on the PPG/RGO/GC electrode and it exhibits the rapidest charge transfer ability among the three electrodes. On the basis of the ratio of the forward anodic peak current density to the backward anodic peak current density in the cyclic voltammograms, the presence of PPG and graphene improved the catalyst tolerance to carbonaceous species accumulation, such as CO, due to the presence of oxygen-containing functional groups in both PPG and graphene, which is proved by IR spectra of the PPG/GC and PPG/RGO/GC electrodes. Both PPG and graphene play an important role in improving Pt particle dispersion and suppressing the agglomeration of Pt particles. In summary, the Pt electrode prepared at −0.25 V and the Pt loading of 250 $\mu g\,cm^{-2}$ have higher electrocatalytic activity, better stability, and improve the catalyst tolerance to CO poisoning.

Acknowledgements

A Project Funded by the Priority Academic Program Development of Jiangsu Higher Education Institutions.

References

[1] X. Ren, P. Zelenay, S. Thomas, J. Davey, S. Gottesfeld, J. Power Sources 86 (2000) 111–116.
[2] V.M. Barragán, A. Heinzel, J. Power Sources 104 (2002) 66–72.
[3] J.W. Guo, T.S. Zhao, J. Prabhuram, R. Chen, C.W. Wong, Electrochim. Acta 51 (2005) 754–763.
[4] F. Kadirgan, S. Beyhan, T. Atilan, Int. J. Hydrogen Energy 34 (2009) 4312–4320.
[5] S.K. Kamarudin, F. Achmad, W.R.W. Daud, Int. J. Hydrogen Energy 34 (2009) 6902–6916.
[6] R.F. Service, Science 296 (2002) 1222–1224.
[7] D.H. Jung, C.H. Lee, C.S. Kim, D.R. Shin, J. Power Sources 71 (1998) 169–173.
[8] W.H.L. Valbuena, V.A. Paganin, C.A.P. Leite, F. Galembeck, Electrochim. Acta 48 (2003) 3869–3878.
[9] H. Yang, T.S. Zhao, Q. Ye, J. Power Sources 139 (2005) 79–90.
[10] K. Makino, K. Furukawa, K. Okajima, M. Sudoh, Electrochim. Acta 51 (2005) 961–965.
[11] A.G. Hubert, M.M. Nenad, N.R.J. Philip, J. Phys. Chem. 99 (1995) 8945–8949.
[12] R.T.S. Oliveira, M.C. Santos, B.G. Marcussi, P.A.P. Nascente, L.O.S. Bulhoes, E.C. Pereira, J. Electroanal. Chem. 575 (2005) 177–182.
[13] H.B. Zhao, J. Yang, L. Li, H. Li, J.L. Wang, Y.M. Zhang, Int. J. Hydrogen Energy 34 (2009) 3908–3914.
[14] Z.H. Wang, G.Q. Gao, H.F. Zhu, Z.D. Sun, H.P. Liu, X.L. Zhao, Int. J. Hydrogen Energy 34 (2009) 9334–9340.
[15] P. Waszczuk, G.Q. Lu, A. Wieckowski, C. Lu, C. Rice, R.I. Masel, Electrochim. Acta 47 (2002) 3637–3652.
[16] A.S. Aricó, P.L. Antonucci, E. Modica, V. Baglio, H. Kim, V. Antonucci, Electrochim. Acta 47 (2002) 3723–3732.
[17] L. Gao, H.L. Huang, C. Korzeniewski, Electrochim. Acta 49 (2004) 1281–1287.
[18] L. Kavan, M. Grätzel, J. Rathousky, A. Zukalb, J. Electrochem. Soc. 143 (1996) 394–400.
[19] A.B. Kashyout, A.B.A.A. Nassr, L. Giorgi, T. Maiyalagan, B.A.B. Youssef, Int. J. Electrochem. Sci. 6 (2011) 379–393.
[20] H.A. Gasteiger, N.M. Markovic, P.N. Ross Jr., J. Phys. Chem. 99 (1995) 8945–8949.
[21] M. Wang, D.J. Guo, H.L. Li, J. Solid State Chem. 178 (2005) 1996–2000.
[22] Y.B. He, G.R. Li, Z.L. Wang, Y.N. Ou, Y.X. Tong, J. Phys. Chem. C 114 (2010) 19175–19181.
[23] H.J. Wang, H. Yu, F. Peng, P. Lv, Electrochem. Commun. 8 (2006) 499–504.
[24] V. Selvaraj, M. Alagar, Electrochem. Commun. 9 (2007) 1145–1153.
[25] C.L. Childers, H.L. Huang, C. Korzeniewski, Langmuir 15 (1999) 786–789.
[26] Z. Jusys, R.J. Behm, J. Phys. Chem. B 105 (2001) 10874–10883.
[27] T. Huang, R.R. Jiang, J.L. Liu, J.H. Zhuang, W.B. Cai, A.S. Yu, Electrochim. Acta 54 (2009) 4436–4440.
[28] S.F. Zhang, J.S. Hu, L.S. Zhong, L.J. Wan, W.G. Song, J. Phys. Chem. C 111 (2007) 11174–11179.
[29] Y.L. Yao, Y. Ding, L.S. Ye, X.H. Xia, Carbon 44 (2006) 61–66.
[30] C. Wang, M. Waje, X. Wang, J.M. Tang, R.C. Haddon, Y.S. Yan, Nano letters 4 (2004) 345–348.
[31] M. Hepel, J. Electrochem. Soc. 145 (1998) 124–134.
[32] V. Selvaraj, M. Alagar, I. Harnerton, J. Power Sources 160 (2006) 940–948.
[33] Z.A. Hu, L.J. Ren, X.J. Feng, Y.P. Wang, Y.Y. Yang, J. Shi, L.P. Mo, Z.Q. Lei, Electrochem. Commun. 9 (2007) 97–102.
[34] F.J. Liu, L.M. Huang, T.C. Wen, A. Gopalan, Synth. Met. 157 (2007) 651–658.
[35] L. Niu, O.H. Li, F.H. Wei, X. Chen, H. Wang, J. Electroanal. Chem. 544 (2003) 121–128.
[36] S.M. Golabi, A. Nozad, A. Nozad, J. Electroanal. Chem. 521 (2002) 161–167.
[37] A.N. Golikand, S.M. Golabi, M.G. Maragheh, L. Irannejad, J. Power Sources 145 (2005) 116–123.
[38] W.Q. Zhou, Y.K. Du, F.F. Ren, C.Y. Wang, J.K. Xu, Int. J. Hydrogen Energy 35 (2010) 3270–3279.
[39] N. Rajalakshmi, H. Ryu, M.M. Shaijumon, S. Ramaprabhu, J. Power Sources 140 (2005) 250–257.
[40] Y.C. Xing, J. Phys. Chem. B 108 (2004) 19255–19259.
[41] H.A. Gasteiger, N. Markovic, P.N. Ross Jr., E.J. Cairns, Electrochim. Acta 39 (1994) 1825–1832.
[42] P. Gouérec, M. Savy, J. Riga, Electrochim. Acta 43 (1997) 743–753.
[43] P. Hernández-Fernández, S. Baranton, S. Rojas, P. Ocón, J.M. Léger, J.L.G. Fierro, Langmuir 27 (2011) 9621–9629.
[44] E. Yoo, T. Okata, T. Akita, M. Kohyama, J. Nakamura, I. Honma, Nano letters 9 (2009) 2255–2259.
[45] N. Shang, P. Papakonstantinou, P. Wang, S.R.P. Silva, J. Phys. Chem. C 114 (2010) 15837–15841.
[46] H. Zhang, X.Q. Xu, P. Gu, C.Y. Li, P. Wu, C.X. Cai, Electrochim. Acta 56 (2011) 7064–7070.
[47] C.A. Bessel, K. Laubernds, N.M. Rodriguez, R.T.K. Baker, J. Phys. Chem. B 105 (2001) 1115–1118.
[48] S.B. Khoo, J. Zhu, Anal. Chim. Acta 373 (1998) 15–27.
[49] M. Zhou, Y.M. Zhai, S.J. Dong, Anal. Chem. 81 (2009) 5603–5613.
[50] W.L. Chen, S.L. Mu, Electrochim. Acta 56 (2011) 2284–2289.
[51] S.L. Mu, Electrochim. Acta 56 (2011) 3764–3772.
[52] W. Hummers, R. Offeman, J. Am. Chem. Soc. 80 (1958) 1339–1340.
[53] J.B. Lambert, H.F. Shurvell, D.A. Lightner, R.G. Cooks, Organic Structural Spectroscopy, Prentice-Hall, Upper Saddle River, NJ, 1998, pp. 224–226.
[54] Z. Jusys, J. Kaiser, R.J. Behm, Langmuir 19 (2003) 6759–6769.
[55] B. Rajesh, K.R. Thampi, J.M. Bonard, A.J. McEvoy, N. Xanthopoulos, H.J. Mathieu, B. Viswanathan, J. Power Sources 133 (2004) 155–161.
[56] Y.H. Lin, X.L. Cui, C. Yen, C.M. Wai, J. Phys. Chem. B 109 (2005) 14410–14415.